Radiation-induced Metabolic Shifts in the Hepatic Parenchyma: Findings from ^{18}F-FDG PET Imaging and Tissue NMR Metabolomics in a Mouse Model for Hepatocellular Carcinoma

Yi-Hsiu Chung
Chang Gung Memorial Hospital, Taiwan
Cheng-Kun Tsai
Clinical Metabolomics Core Lab, Chang Gung Memorial Hospital at Linkou
Ching-Fang Yu
Radiation Biology Research Center, Institution for Radiological Research
Wan-Ling Wang
Department of Nuclear Medicine, Chang Gung Memorial Hospital
Chung-Lin Yang
Department of Medical Imaging and Radiological Sciences, Chang Gung Memorial Hospital
Ji-Hong Hong
Department of Radiation Oncology, Chang Gung Memorial Hospital
Tzu-Chen Yen
Department of Nuclear Medicine, Chang Gung Memorial Hospital
Fang-Hsin Chen
Department of Medicine Imaging and Radiological Sciences, Chang Gung Memorial Hospital
Gigin Lin (giginlin@cgmh.org.tw)
Chang Gung Memorial Hospital and Chang Gung University, Linkou Medical Center, 5 Fuhsing Street, Guishan, Taoyuan 333, Taiwan https://orcid.org/0000-0001-7246-1058

Original research

Keywords: Radiation, liver cancer, 18FDG-PET, glycolysis, NMR

Posted Date: November 3rd, 2020

DOI: https://doi.org/10.21203/rs.3.rs-99645/v1

Version of Record: A version of this preprint was published at Molecules on April 28th, 2021. See the published version at https://doi.org/10.3390/molecules26092573.

Abstract

Purpose: By taking advantage of ^{18}F-FDG PET imaging and tissue nuclear magnetic resonance (NMR) metabolomics, we examined the dynamic metabolic alterations induced by liver irradiation in a mouse model for hepatocellular carcinoma (HCC).

Methods: After orthotopic implantation with the mouse liver cancer BNL cells in the right hepatic lobe, animals were divided into two experimental groups. The first received irradiation (RT) at 15 Gy whereas the second (no-RT) did not. Intergroup comparisons over time were performed in terms of ^{18}F-FDG PET findings, NMR metabolomics results, and expression of genes involved in inflammation and glucose metabolism.

Results: As of day 1 post-irradiation, mice in the RT group showed an increased ^{18}F-FDG uptake in the right liver parenchyma compared with the no-RT group. However, the difference reached statistical significance only on the third post-irradiation day. NMR metabolomics revealed that glucose concentrations peaked on day 1 post-irradiation both in the right and left lobes – the latter reflecting a bystander effect. Increased pyruvate and glutamate levels were also evident in the right liver on the third post-irradiation day. The expression levels of the glucose-6-phosphatase (*G6PC*) and fructose-1, 6-bisphosphatase 1 (*FBP1*) genes were down-regulated on the first and third post-irradiation days, respectively. Thus, liver irradiation was associated with a metabolic shift from an impaired gluconeogenesis to an enhanced glycolysis from the first to the third post-irradiation day.

Conclusion: Radiation-induced metabolic alterations in the liver parenchyma occur as early as the first post-irradiation day and show dynamic changes over time.

Introduction

Hepatocellular carcinoma (HCC) is the sixth most common cancer worldwide [1, 2]. While radiotherapy is an integral part of current HCC treatment protocols, radiation-induced liver disease (RILD) continues to represent a major obstacle to its widespread implementation [3, 4]. The onset of RILD is clinically characterized by anicteric hepatomegaly, ascites, and elevated serum alkaline phosphatase. Conversely, atypical signs include jaundice as well as elevated transaminase levels – including aspartate aminotransferase (AST) and alanine aminotransferase (ALT) [5]. The onset of RILD in humans generally occurs 3 – 6 months after liver irradiation, whereas it traditionally appears at two post-irradiation weeks in rodent models [5, 6]. In this context, an in-depth knowledge of early metabolic changes occurring in the liver as a result of irradiation is paramount to shed further light on the pathophysiology of RILD.

Positron emission tomography (PET) with 2-deoxy-2-[18F]fluoro-D-glucose (^{18}F-FDG) has several key applications in the field of oncology – including diagnosis, tumor staging, and assessment of treatment response [7]. The basic principle underlying this technique lies in its ability to measure glucose uptake [8–10]. However, areas of infection or active inflammation may lead to false positive results in up to 13% of

all cases [11]. It can be speculated that the increased ^{18}F-FDG uptake in patients with HCC who develop RILD may at least in part stem from inflammatory and/or metabolic mechanisms. Tissue nuclear magnetic resonance (NMR) metabolomics is increasingly being applied as an analytical platform to identify and quantify metabolites under different biological conditions [12, 13]. We therefore reasoned that this technique would allow extensive analysis of glucose metabolic pathways in irradiated liver samples – ultimately improving our understanding of RILD pathophysiology.

By taking advantage of ^{18}F-FDG PET imaging and tissue NMR metabolomics, we therefore designed the current study to investigate the metabolic alterations associated with liver irradiation in a mouse model for HCC.

Materials And Methods

Experimental design

At day 10 after implantation of mouse liver cancer BNL cells in the right lobe of the liver, mice underwent T2-weighted magnetic resonance (MR) imaging to determine tumor size. Subsequently, animals were randomly divided into two experimental groups. The irradiation (RT) group consisted of five mice which underwent partial irradiation (15 Gy) of the right liver lobe on the day of MR imaging. The no-RT group comprised five mice which were not irradiated. ^{18}F-FDG PET scans were performed in the pre-irradiation phase (day 0) as well as on days 1 and 3 post-irradiation. *Ex vivo* NMR metabolomics experiments were carried out on tumor and normal liver parenchyma samples on days 1 and 3 post-irradiation (n = 6 for both groups). Serum ALT and AST levels were measured on a biochemical analyzer in both the RT (on days 1 and 3 post-irradiation) and no-RT groups. *Ex vivo* immunochemical staining of inflammatory markers was performed on day 3 post-irradiation. The hepatic expression of the following genes was also assessed by qPCR in the post-irradiation phase: 1) genes involved in glucose metabolism – including phosphoenolpyruvate carboxykinase 1 (*PCK1*), fructose bisphosphatase 1 (*FBP1*), glucose-6-phosphatase (*G6PC*), and pyruvate carboxylase (*PC*); 2) hypoxia induced factor 1, alpha subunit (HIF-1α), and 3) genes involved in inflammation – including interleukin (IL)-18, IL-1β, and IL-6. Figure 1 depicts the experimental flow of the study.

Animal model and procedures for irradiation

Ethical approval for all animal experiments was received from the Institutional Animal Care and Use Committee of the National Tsing Hua University (approval number: 10414) and the Chang Gung Memorial Hospital (approval number: 2016010701). The animal model and the procedures used for irradiation have been previously described in detail [14]. In brief, mouse liver cancer BNL cells (1×10^5 cells suspended in 20 µL of HBSS) were orthotopically implanted with a 30-G needle in the right liver lobe of 8-week-old male Balb/c mice. Before irradiation, mice were put under general anesthesia with a mixture (1:1) of ketamine (50 mg/mL) and 1% xylazine and restrained using an adhesive tape. Subsequently, the

right liver was partially irradiated with 6-MV X-ray beams (15 Gy) obtained from a clinical linear accelerator.

^{18}F-FDG PET/CT imaging protocol and analysis

^{18}F-FDG PET/CT whole-body scans obtained from experimental animals were retrospectively retrieved from the dataset used for our previous study [14]. In brief, mice underwent computed tomography (CT) using ExiTron™ nano6000 (0.1 mL) as contrast agent. Within one hour, they were subjected to ^{18}F-FDG PET imaging after the injection of ^{18}F-FDG (8.1 MBq). PET and CT images were acquired on the same animal bed using the Inveon™ (Siemens Medical Solutions Inc., Malvern, PA, USA) and the NanoSPECT/CT (Mediso Kft., Budapest, Hungary) systems, respectively. The volumes of interest (VOIs) within the liver parenchyma were manually identified on PET/CT fused images. The upper portion of the left liver lobe was not included in VOIs identification because of the spillover from myocardium or myocardial motion. As for VOIs definition in the right liver parenchyma, caution was exercised as to avoid the inclusion of both the tumor area and extrahepatic regions. The standardized uptake value (SUV) was calculated by multiplying lesion concentration of the tracer by the animal body weight divided by the injected dose. Image analysis was carried out with PMOD version 4.0 (PMOD Technologies Ltd., Zurich, Switzerland).

Collection and extraction of the liver tissue for NMR metabolomics

Mice in the RT and no-RT groups (n = 6 each) were anesthetized as described above before undergoing portal vein perfusion. Samples were removed bilaterally from the liver parenchyma and stored (100 µg each) at -80 °C in CryoTube™ vials (1.8 mL; Thermo Fisher Scientific, Waltham, MA, USA). Aqueous extracts were resuspended in a buffer (650 µL) containing 0.008% trisodium phosphate, 7.5 mM Na_2HPO_4, 0.2 mM NaN_3, and 92% D_2O. After centrifugation at 4 °C for 5 min, sample supernatants (600 µL) were withdrawn in SampleJet NMR tubes (Bruker, Billerica, MA, USA).

NMR metabolomics data processing

NMR metabolomics analyses were conducted on a Bruker AVANCE III HD System equipped with a 14.1-T magnet running at 600 MHz (1H NMR) and 279 K. NMR spectra were acquired with the following pulse sequences: noesygppr1d, cpmgpr1d, and zg30. Metabolite profiles were identified and analyzed using the Chenomx NMR Suite 8.4 professional software (Chenomx Inc., Edmonton, Alberta, Canada). The frequency position of tetramethylsilane (TMS) resonance was defined as exactly 0.0 ppm, and the concentrations of each metabolite were calculated after normalization for the area of the reference TMS sample. Raw data were analyzed using the build-in principal component analysis (PCA) and partial least squares discriminant analysis (PLS-DA) packages available from the MetaboAnalyst 3.0 website (www.metabonanlyst.ca). We used the Variable Importance in Projection (VIP) values to express the

contribution of each metabolite to the PLS-DA model. A p value < 0.05 and a VIP score > 1.1 were considered as significant.

Serum biomarkers of liver damage

Blood samples were collected from experimental animals in tubes coated with lithium heparin (AmiShield, Taoyuan, Taiwan) on days 1, 3, and 6 post-RT. Serum was isolated by centrifugation at 1500 rpm for 10 min. Quantification of AST, ALT, and albumin was carried out on a biochemical analyzer (AmiShield) according to the manufacturer's protocol.

Immunohistochemical staining of inflammatory markers

Mice were sacrificed at day 3 post-RT and tissues were embedded in the optimal cutting temperature compound for cryosection. Immunohistochemical staining was performed as previously described [14]. CD68 and F4/80 antibodies (Bio-Rad, Hercules, CA, USA) were used as macrophage markers. Results of immunostaining were quantified with the Image-Pro Plus software (Media Cybernetics, Silver Spring, MD, USA).

RNA extraction and gene expression analysis

Mice were sacrificed at day 3 post-RT and liver tissue samples were stored in liquid nitrogen. Total RNA extracted from normal tissue of the right and left lobes of the liver was isolated using the TRIzol reagent and reverse transcribed to cDNA with the Omniscript reverse transcriptase kit (Qiagen, Hilden, Germany). Quantitative PCR reactions were carried out with the LightCycler® 480 SYBR Green I Master reagent (Roche Diagnostics Corporation, Indianapolis, IN, USA), and subsequently analyzed using the CFX Connect™ Real-Time PCR Detection System (Bio-Rad). The primer sequences are shown in Supplement File 1.

Statistical analysis

Continuous data are expressed as means ± standard deviations (SDs). Groups were compared on hepatic SUVs values with the Student's *t*-test. Variables obtained from NMR metabolomics experiments were analyzed with the Student's *t*-test, one-way analysis of variance (ANOVA), or the chi-square test, as appropriate. As for qPCR data, changes in expression for each of the investigated genes were determined by calculating the ΔΔCt values and compared with unpaired Student's *t*-tests. All analyses were carried out in GraphPad Prism 6 (GraphPad Inc., San Diego, CA, USA). Statistical significance was determined by a two-tailed p value < 0.05.

Results

^{18} F-FDG uptake in irradiated and not-irradiated liver parenchyma

^{18}F-FDG PET/CT scans were conducted on post-RT days 1 and 3 to monitor the ^{18}F-FDG uptake in the liver parenchyma of mice bearing experimental HCC. Animals in the no-RT group served as controls. Representative transaxial planes of liver CT and ^{18}F-FDG PET/CT images obtained in the two experimental groups are shown in Fig. 2a. On post-RT day 1, a mildly increased ^{18}F-FDG uptake was observed in the right liver parenchyma of irradiated mice. On post-RT day 3, the ^{18}F-FDG uptake in the right liver parenchyma was significantly higher in the irradiated group compared with the non-irradiated group (SUVmax: 1.06 ± 0.29 *versus* 0.66 ± 0.08, respectively, $p < 0.01$; SUVmean: 0.71 ± 0.13 *versus* 0.49 ± 0.04, respectively, $p < 0.05$; Fig. 2b). In experiments conducted in tumor-free animals, the right-to-left ratio of ^{18}F-FDG uptake in the liver parenchyma measured on post-RT day 3 was 1.13-fold higher in the RT group compared with the no-RT group (1.11 ± 0.10 *versus* 0.98 ± 0.03, respectively, $p < 0.05$).

Metabolic changes in irradiated and not-irradiated liver parenchyma

On post-RT day 3, PCA plots revealed significant differences with respect to metabolite concentrations in the right liver of mice in the RT and no-RT groups (Fig. 3) – which were not evident for the left lobe. In addition, no significant differences were observed between the right and left lobes of the liver on post-RT day 1. Changes in expression of each metabolite in the RT and no-RT groups are summarized in Table 1. On post-RT day 1, significant increases in the following metabolites were observed in the left liver lobe: alanine, anserine, galactarate, galactitol, glucose, glycylproline, malonate, N-methylhydantoin, and succinate ($p < 0.05$). As for the right liver lobe, significant increases on post-RT day 1 were evident for galactarate, galactitol, glucose, and sucrose ($p < 0.05$). Among different metabolites, the highest elevation was observed for glucose (18- and 17-fold in the left and right liver, respectively). On post-RT day 3, the only metabolite found to be significantly increased in the left liver lobe was fumarate. Other metabolites were decreased, albeit not significantly so. While significant elevations of glutamate, pyruvate, and sucrose were observed in the right liver, other metabolites were significantly decreased.

Table 1
Dynamic changes in the expression of different metabolites in the right and left lobes of the liver observed in the two study groups on the first and third post-irradiation days.

Metabolite	VIP score	Fold change (|RT/no-RT |>1.1)	P	Metabolite	VIP score	Fold change (|RT/no-RT| >1.1)	P
Right liver		**Day 1**				**Day 3**	
Glucose	3.456	16.930	0.003	Pyruvate	1.818	6.996	0.008
Sucrose	2.244	13.483	0.015	Glutamate	1.043	3.487	0.024
Galactarate	1.396	2.523	0.003	Sucrose	1.153	2.812	0.019
Galactitol	1.931	4.776	0.001	Malonate	0.879	0.565	1.6E-04
				Pyridoxine	0.836	0.512	0.006
				Choline	0.955	0.479	0.009
				Niacinamide	1.244	0.345	1.7E-07
				Hypoxanthine	1.763	0.341	0.028
				Betaine	1.449	0.252	1.4E-04
				Guanidoacetate	2.690	0.121	0.001
				Sarcosine	1.992	0.090	3.8E-04
				Glycocholate	2.190	0.059	2.0E-04
Left liver		**Day 1**				**Day 3**	
Glucose	2.561	17.774	0.008	Fumarate	1.108	1.844	0.001
Malonate	2.597	9.836	0.001	Niacinamide	0.981	0.577	0.005
Succinate	2.437	3.979	0.004	Riboflavin	1.062	0.452	0.029
Galactitol	1.539	3.506	0.001	Succinate	1.200	0.428	0.008
Glycylproline	1.350	3.018	1.7E-04	Succinylacetone	1.326	0.415	0.043
Galactarate	1.404	2.866	0.001	Betaine	1.492	0.364	3.2E-04

Metabolite	VIP score	Fold change (|RT/no-RT|>1.1)	P	Metabolite	VIP score	Fold change (|RT/no-RT|>1.1)	P
Alanine	1.185	2.093	0.018	Sarcosine	1.448	0.349	0.002
N-Methylhydantoin	0.919	1.832	0.049	Guanidoacetate	2.401	0.335	0.036
Anserine	0.613	1.433	0.046				

Markers of inflammation and gluconeogenesis in irradiated and not-irradiated liver parenchyma

We have previously shown that local irradiation induces a continuous influx of macrophages at sites of orthotopic hepatic neoplasms [14] – which was in turn associated with a higher tumor ^{18}F-FDG uptake. Herein, we have shown that ^{18}F-FDG uptake is increased in normal hepatic tissue on post-RT day 3. Nonetheless, there was no significant expansion of CD8 + T cells as well as of the F4/80 + or CD68 + macrophage populations in liver tissues on post-RT days 1 and 3 (data not shown). Taken together, these results indicate that the radiation-induced increase in ^{18}F-FDG uptake in the liver is not related to an enhanced infiltration of immune cells. Analyses of pro-inflammatory cytokines revealed a mild increase in IL-18 expression and a significant increase in IL-6 expression in the right liver of irradiated mice on post-RT day 3 (Fig. 4, $p < 0.05$). Differences were also observed with respect of both IL-1β and HIF-1α in the right liver of irradiated mice on post-RT days 1 and 3. In the left lobe of irradiated mice, we found an overexpression of IL-18 and IL-6 on post-RT day 1 and of HIF-1α, IL-1β, and IL-6 on post-RT day 3. We speculate that this phenomenon may stem from a bystander effect as only the right portion of the liver was directly irradiated (Supplement File 2). The results of qPCR conducted in extracts from right liver tissues revealed a reduction of *G6PC* gene in irradiated tissue compared with non-irradiated tissue on post-RT day 1. Similarly, expression levels of the *FPB1* gene were significantly lower in irradiated tissue compared with non-irradiated tissue on post-RT day 3 (Fig. 5).

Assessment of liver enzymes in irradiated mice bearing orthotopic HCC

The extent of liver damage was assessed by measuring serum levels of AST, ALT, and albumin. Compared with control animals, the presence of experimental tumors resulted in increased ALT (36.4 ± 11.00 *versus* 52.67 ± 8.08 IU/L, respectively, $p = 0.021$) and albumin levels (1.36 ± 0.50 g/dL *versus* 3.27 ± 0.15 g/dL, respectively, $p < 0.0001$). However, ALT and albumin levels did not show significant differences in the RT and no-RT groups on post-RT days 1 and 6. These results indicate that irradiation *per se* does

not increase AST and albumin levels. Consequently, these indices cannot serve as reliable biomarkers of radiation-induced liver damage in tumor-bearing mice.

Alterations in hepatic metabolic pathways in response to irradiation

In the right portion of the liver, the following metabolic pathways were found to be altered on post-RT day 1: starch and sucrose metabolism, galactose metabolism, and biosynthesis of neomycin, kanamycin, and gentamicin. On post-RT day 3, increased pyruvate and glutamate levels were associated with alterations in the metabolism of several amino acids – including D-glutamine-D-glutamate metabolism, alanine-aspartic acid-glutamic acid metabolism, glycine-serine-threonine metabolism, and arginine-proline metabolism. The metabolic changes predicted by the MetaboAnalyst 3.0 platform for the right and left lobes of the liver on post-RT days 1 and 3 are shown in Supplement File 3. By taking into account the results of ^{18}F-FDG PET/CT imaging, NMR metabolomics, and qPCR, we formulated a theoretical model for radiation-induced metabolic alterations in the right liver on post-RT days 1 and 3 – according to which gluconeogenesis and glycolysis were alternatively affected (Fig. 6).

Discussion

Using an animal model, herein we show that liver irradiation results in a precise temporal sequence of metabolic alterations in the hepatic parenchyma – which was characterized by an alternate pattern (e.g., early inhibition of gluconeogenesis followed by a switch to glycolysis). Notably, we also provide evidence that ^{18}F-FDG PET/CT imaging may serve as a useful surrogate tool for monitoring the occurrence and temporal course of metabolic changes elicited by hepatic irradiation. Differently from ^{18}F-FDG PET/CT, common biochemical indices of hepatocyte damage – including AST, ALT, and albumin – did not serve as useful markers for radiation-induced liver damage.

The enhanced ^{18}F-FDG uptake observed in the RT group on post-RT day 3 was likely the result of an increased release of IL-6 – a well-known pro-inflammatory cytokine. Conversely, immune cell infiltration did not appreciably increase in the irradiated liver parenchyma – ultimately suggesting that immune cells were not directly responsible for the increased ^{18}F-FDG avidity in the post-irradiation phase. Apart from gluconeogenesis and glycolysis, fatty acid biosynthesis and amino acid metabolism were identified as the mostly affected metabolic pathways. All of them were found to be altered both in the irradiated right liver and in the contralateral non-irradiated lobe. Intriguingly, the increased ^{18}F-FDG uptake was accompanied by an increased pyruvate-to-glutamate ratio and a reduced expression of the *FBP1* gene in the irradiated liver. Altogether, these results point to an enhanced glycolysis as the metabolic milieu underlying the enhanced ^{18}F-FDG avidity at three days post-irradiation. A previous study reported that the biological damage observed in rats following total body irradiation (8 Gy) peaked after 72 hours [15]. In accordance with our research, the authors identified radiation-induced alterations in amino acid metabolism – specifically involving the glycine-serine-threonine and the alanine-aspartate-glutamine

pathways [15]. Our results may pave the way to the use of radiation-induced alterations in hepatic metabolism as promising biomarkers for monitoring the occurrence and progression of RILD.

Metabolic switch to glycolysis following irradiation of the liver parenchyma

While hepatic gluconeogenesis leads to the synthesis of glucose, glycolysis is an energy production pathway during which one glucose molecule is split into two pyruvate molecules [16]. Previous animal studies have shown that hyperglycemia and increased glycogen stores in the liver can be observed in the early post-irradiation phase – indicating a key role for gluconeogenesis in early radiation response [17, 18]. Another study reported a decreased glycolysis in mice subjected to whole liver irradiation (10 Gy) on post-RT day 1 [19]. The increased amount of glucose detected in our NMR metabolomics experiments is in keeping with the published literature and – consistently – hepatic ^{18}F-FDG uptake was not significantly increased on post-RT day 1. The increased amount of glucose in the liver parenchyma may in turn inhibit *G6PC* gene expression, lending further support to the inhibition of gluconeogenesis within the first post-irradiation day. However, hepatic glucose metabolism was found to change dramatically on post-RT day 3. By that time, the enhanced hepatic ^{18}F-FDG uptake, the increased detection of pyruvate, and the decreased expression of the *FBP1* gene concordantly suggested that a switch to glycolysis had occurred. Activation of glycolysis can be reflected by an increased in both up-stream metabolites (i.e., glucose and sucrose) and the final down-stream product (i.e., pyruvate) [20]. Taken together, these results indicate that early and delayed alterations in glucose metabolism merit further investigation and scrutiny as promising biomarkers of RILD [21, 22]. Whether manipulation of glucose metabolism before or immediately after irradiation may result in a decreased production of reactive oxygen species (ROS) and/or proinflammatory molecules remains to be established [23–25].

Inflammatory response in irradiated liver parenchyma

Radiation is known to induce a proinflammatory tissue response, and there is evidence that IL-6 and NF-kB are among the key molecular mediators of RILD [26]. Moreover, proinflammatory mechanisms have been advocated to explain the increased^{18}F-FDG avidity observed in liver and lung tissues of mice subjected to experimental irradiations [27]. While we did not observe an increased hepatic infiltration of immune cells on post-RT days 1 and 3, the expression of IL-6 in the right liver increased gradually over time. Notably, IL-6 can stimulate glycolysis within the tumor microenvironment [28] and a disturbed glucose metabolism can elicit proinflammatory effects [29–31]. The complex interplays between radiation-induced alterations in glucose metabolism and inflammatory mechanisms should be subject to future research.

Bystander effects in the left liver lobe

Although only the right liver lobe was directly irradiated in our study, alterations affecting the tricarboxylic acid cycle, the biosynthesis of fatty acids, and amino acid metabolism were also observed in the left hepatic lobe on post-RT days 1 and 3. These metabolic changes – which were accompanied by

significantly increased expression of IL-18 and IL-6 on day 1 as well as of IL-1β, HIF-1α, and IL-6 on day 3 – are likely the results of a bystander effect. Radiation-induced ROS production elicits the release of pro-inflammatory cytokines [25]. Previous studies have shown that the bystander effect occurring in hepatoma cells irradiated with α-particles was mediated by ROS through a p53-dependent pathway [32, 33]. Another study conducted in a rat model reported the occurrence of a bystander effect in the brain (with altered gene expression and evidence of DNA damage) following irradiation of the liver [34]. The bystander metabolic changes in the left liver lobe observed in the current study may stem from paracrine effects elicited by proinflammatory cytokines released from the irradiated right lobe [35].

Future research directions

Radiation-induced ROS generation is deemed to play a critical role in determining liver radiosensitivity. Interestingly, a blunted hepatic pyruvate dehydrogenase complex activity has been associated with a reduced production of ROS [23, 36]. Future research should address whether specific manipulation of gluconeogenesis and/or glycolysis might reduce the sensitivity of the liver parenchyma to radiation therapy through a modulation of ROS formation.

Conclusions

The results of the current study demonstrate that experimental irradiation of the liver parenchyma results in dynamic metabolic changes that were detectable by different techniques (^{18}F-FDG PET/CT imaging, NMR metabolomics, and qPCR) as early as 1 day post-RT. These findings have important clinical implications concerning the use of ^{18}F-FDG PET/CT for monitoring patients with HCC treated with radiotherapy. Specifically, the increased uptake of ^{18}F-FDG in this clinical population may at least in part reflect an enhanced glycolysis as an expression of radiation-induced alterations in the hepatic parenchyma. We conclude that ^{18}F-FDG PET/CT should be used with caution in this clinical setting as it can yield false-positive results and may lead to erroneous estimates of tumor margins.

Declarations

Ethics approval and consent to participate

Ethical approval for all animal experiments was received from the Institutional Animal Care and Use Committee of the National Tsing Hua University (approval number: 10414) and the Chang Gung Memorial Hospital (approval number: 2016010701).

Consent for publication

Not applicable

Availability of data and material

The datasets used and/or analysed during the current study are available from the corresponding author on reasonable request.

Competing interests

The authors declare that they have no competing interests

Funding

This work was supported by grants from the Chang Gung Medical Foundation (CMRPD1H0473, CMRPD1J0322, CRRPG3K1341, CMRPG3B0313 and CLRPG3K0021) and the Taiwan Ministry of Science and Technology (MOST 109-2628-B-182-008 to Fang-Hsin Chen; MOST 106-2627-M-182A-002 to Tzu-Chen Yen; and MOST 109-2628-B-182A-007 to Gigin Lin).

Authors' contributions

Yi-Hsiu Chung, Cheng-Kun Tsai, and Ching-Fang Yu contributed equally to this work. Organize and analyze all data. Yi-Hsiu Chung carried out the imaging section and drafted the manuscript. Cheng-Kun Tsai participated metabolic data analysis. Ching-Fang Yu carried out animal model surgery and biochemistries work including IHC staining, immunoassays and serum enzyme test, etc. Wan-Ling Wang and Chung-Lin Yang carried out liver metabolite extraction and perfused liver tissue work. Ji-Hong Hong and Tzu-Chen Yen provides funding supporting and supervised this project. Fang-Hsin Chen and Gigin Lin are co-corresponding authors, participating in the study design and coordination the helped to draft the manuscript.

Acknowledgements

We acknowledge Radiation Biology Core Laboratory, Chang Gung Memorial Hospital, for irradiation support and immunohistochemistry image capture, and Center for Advanced Molecular Imaging and Translation, Chang Gung Memorial Hospital, for imaging support, and Clinical Metabolomics Core Lab, Chang Gung Memorial Hospital, for metabolite analyses.

Disclosures

The authors declare that there are no conflicts of interest regarding the publication of this paper.

References

1. Torre LA, Bray F, Siegel RL, Ferlay J, Lortet-Tieulent J, Jemal A. Global cancer statistics, 2012. CA Cancer J Clin. 2015;65:87-108. doi:10.3322/caac.21262.
2. Chen DS. Hepatocellular carcinoma in Taiwan. Hepatol Res. 2007;37 Suppl 2:S101-5. doi:10.1111/j.1872-034X.2007.00170.x.

3. Benson R, Madan R, Kilambi R, Chander S. Radiation induced liver disease: A clinical update. J Egypt Natl Canc Inst. 2016;28:7-11. doi:10.1016/j.jnci.2015.08.001.
4. Kim J, Jung Y. Radiation-induced liver disease: current understanding and future perspectives. Exp Mol Med. 2017;49:e359. doi:10.1038/emm.2017.85.
5. Lawrence TS, Robertson JM, Anscher MS, Jirtle RL, Ensminger WD, Fajardo LF. Hepatic toxicity resulting from cancer treatment. Int J Radiat Oncol Biol Phys. 1995;31:1237-48. doi:10.1016/0360-3016(94)00418-K.
6. Cheng W, Xiao L, Ainiwaer A, Wang Y, Wu G, Mao R, et al. Molecular responses of radiation-induced liver damage in rats. Mol Med Rep. 2015;11:2592-600. doi:10.3892/mmr.2014.3051.
7. Norregaard K, Jorgensen JT, Simon M, Melander F, Kristensen LK, Bendix PM, et al. 18F-FDG PET/CT-based early treatment response evaluation of nanoparticle-assisted photothermal cancer therapy. PLoS One. 2017;12:e0177997. doi:10.1371/journal.pone.0177997.
8. Agrawal A, Rangarajan V. Appropriateness criteria of FDG PET/CT in oncology. Indian J Radiol Imaging. 2015;25:88-101. doi:10.4103/0971-3026.155823.
9. Kinahan PE, Fletcher JW. Positron emission tomography-computed tomography standardized uptake values in clinical practice and assessing response to therapy. Semin Ultrasound CT MR. 2010;31:496-505. doi:10.1053/j.sult.2010.10.001.
10. Kiyohara S, Nagamachi S, Wakamatsu H, Nishii R, Fujita S, Futami S, et al. [Usefulness of metabolic volume and total lesion glycolysis for predicting therapeutic response in cancer therapy by 18F-FDG PET/CT]. Kaku Igaku. 2010;47:453-61.
11. Gupta NC, Graeber GM, Bishop HA. Comparative efficacy of positron emission tomography with fluorodeoxyglucose in evaluation of small (<1 cm), intermediate (1 to 3 cm), and large (>3 cm) lymph node lesions. Chest. 2000;117:773-8. doi:10.1378/chest.117.3.773.
12. Dona AC, Kyriakides M, Scott F, Shephard EA, Varshavi D, Veselkov K, et al. A guide to the identification of metabolites in NMR-based metabonomics/metabolomics experiments. Comput Struct Biotechnol J. 2016;14:135-53. doi:10.1016/j.csbj.2016.02.005.
13. Xia J, Sinelnikov IV, Han B, Wishart DS. MetaboAnalyst 3.0–making metabolomics more meaningful. Nucleic Acids Res. 2015;43:W251-7. doi:10.1093/nar/gkv380.
14. Chung YH, Yu CF, Chiu SC, Chiu H, Hsu ST, Wu CR, et al. Diffusion-weighted MRI and (18)F-FDG PET correlation with immunity in early radiotherapy response in BNL hepatocellular carcinoma mouse model: timeline validation. Eur J Nucl Med Mol Imaging. 2019;46:1733-44. doi:10.1007/s00259-019-04318-3.
15. Zhang Y, Zhou X, Li C, Wu J, Kuo JE, Wang C. Assessment of early triage for acute radiation injury in rat model based on urinary amino acid target analysis. Mol Biosyst. 2014;10:1441-9. doi:10.1039/c3mb70526a.
16. Adeva-Andany MM, Perez-Felpete N, Fernandez-Fernandez C, Donapetry-Garcia C, Pazos-Garcia C. Liver glucose metabolism in humans. Biosci Rep. 2016;36. doi:10.1042/BSR20160385.

17. Paulikova E, Ahlers I, Praslicka M. Gluconeogenesis in lethally X-irradiated rats. Physiol Bohemoslov. 1983;32:73-9.
18. Kay RE, Entenman C. Hyperglycemia and increased liver glycogen in rats after x-irradiation. Proc Soc Exp Biol Med. 1956;91:143-6. doi:10.3181/00379727-91-22192.
19. Kurland IJ, Broin PO, Golden A, Su G, Meng F, Liu L, et al. Integrative Metabolic Signatures for Hepatic Radiation Injury. PLoS One. 2015;10:e0124795. doi:10.1371/journal.pone.0124795.
20. Ferreira SJ, Sonnewald U. The mode of sucrose degradation in potato tubers determines the fate of assimilate utilization. Front Plant Sci. 2012;3:23. doi:10.3389/fpls.2012.00023.
21. Wang Z, Dong C. Gluconeogenesis in Cancer: Function and Regulation of PEPCK, FBPase, and G6Pase. Trends Cancer. 2019;5:30-45. doi:10.1016/j.trecan.2018.11.003.
22. Grasmann G, Smolle E, Olschewski H, Leithner K. Gluconeogenesis in cancer cells - Repurposing of a starvation-induced metabolic pathway? Biochim Biophys Acta Rev Cancer. 2019;1872:24-36. doi:10.1016/j.bbcan.2019.05.006.
23. Mossenta M, Busato D, Dal Bo M, Toffoli G. Glucose Metabolism and Oxidative Stress in Hepatocellular Carcinoma: Role and Possible Implications in Novel Therapeutic Strategies. Cancers (Basel). 2020;12. doi:10.3390/cancers12061668.
24. Wei J, Wang H, Wang H, Wang B, Meng L, Xin Y, et al. The role of NLRP3 inflammasome activation in radiation damage. Biomed Pharmacother. 2019;118:109217. doi:10.1016/j.biopha.2019.109217.
25. Xiao M. The Role of Proinflammatory Cytokine Interleukin-18 in Radiation Injury. Health Phys. 2016;111:212-7. doi:10.1097/HP.0000000000000494.
26. Cha H, Lee EJ, Seong J. Multi-analyte analysis of cytokines that predict outcomes in patients with hepatocellular carcinoma treated with radiotherapy. World J Gastroenterol. 2017;23:2077-85. doi:10.3748/wjg.v23.i11.2077.
27. Kesner AL, Lau VK, Speiser M, Hsueh WA, Agazaryan N, DeMarco JJ, et al. Time-course of effects of external beam radiation on [18F]FDG uptake in healthy tissue and bone marrow. J Appl Clin Med Phys. 2008;9:2747. doi:10.1120/jacmp.v9i3.2747.
28. Ando M, Uehara I, Kogure K, Asano Y, Nakajima W, Abe Y, et al. Interleukin 6 enhances glycolysis through expression of the glycolytic enzymes hexokinase 2 and 6-phosphofructo-2-kinase/fructose-2,6-bisphosphatase-3. J Nippon Med Sch. 2010;77:97-105. doi:10.1272/jnms.77.97.
29. Basu A, Shah P, Nielsen M, Basu R, Rizza RA. Effects of type 2 diabetes on the regulation of hepatic glucose metabolism. J Investig Med. 2004;52:366-74. doi:10.1136/jim-52-06-30.
30. Tappy L, D'Alessio D. How are we going to understand (dys)regulation of glucose metabolism? Curr Opin Clin Nutr Metab Care. 2004;7:467-9.
31. Wu Y, Wu T, Wu J, Zhao L, Li Q, Varghese Z, et al. Chronic inflammation exacerbates glucose metabolism disorders in C57BL/6J mice fed with high-fat diet. J Endocrinol. 2013;219:195-204. doi:10.1530/JOE-13-0160.

32. Li J, He M, Shen B, Yuan D, Shao C. Alpha particle-induced bystander effect is mediated by ROS via a p53-dependent SCO2 pathway in hepatoma cells. Int J Radiat Biol. 2013;89:1028-34. doi:10.3109/09553002.2013.817706.
33. Wang X, Zhang J, Fu J, Wang J, Ye S, Liu W, et al. Role of ROS-mediated autophagy in radiation-induced bystander effect of hepatoma cells. Int J Radiat Biol. 2015;91:452-8. doi:10.3109/09553002.2015.1012308.
34. Kovalchuk A, Mychasiuk R, Muhammad A, Hossain S, Ilnytskyy S, Ghose A, et al. Liver irradiation causes distal bystander effects in the rat brain and affects animal behaviour. Oncotarget. 2016;7:4385-98. doi:10.18632/oncotarget.6596.
35. Azzam EI, Jay-Gerin JP, Pain D. Ionizing radiation-induced metabolic oxidative stress and prolonged cell injury. Cancer Lett. 2012;327:48-60. doi:10.1016/j.canlet.2011.12.012.
36. Jeoung NH. Pyruvate Dehydrogenase Kinases: Therapeutic Targets for Diabetes and Cancers. Diabetes Metab J. 2015;39:188-97. doi:10.4093/dmj.2015.39.3.188.

Figures

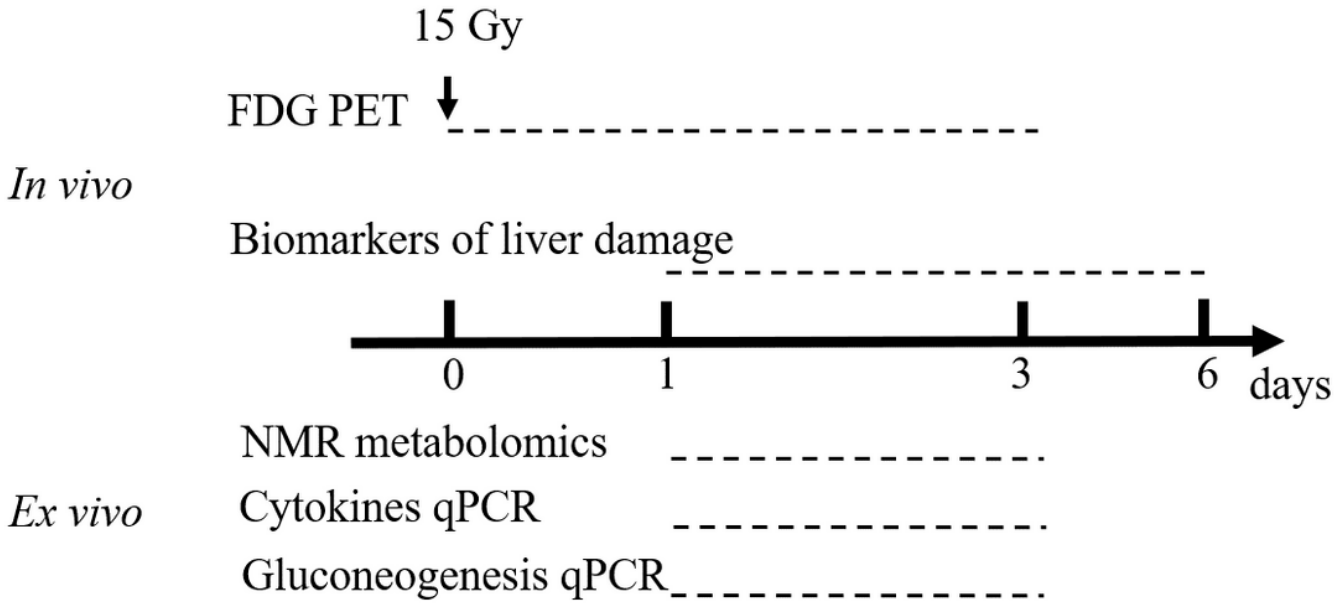

Figure 1

Schematic representation of the experimental workflow. 18F-FDG PET imaging studies of a mouse model for hepatocellular carcinoma were conducted from baseline (i.e., before experimental irradiation) to the

third post-irradiation day. Measurements of biochemical markers of liver damage (ALT, AST, and albumin) were carried out on the first, third, and sixth post-irradiation days. Ex vivo tissue analyses – comprising NMR metabolomics and qPCR experiments – were performed on the first and third post-irradiation days.

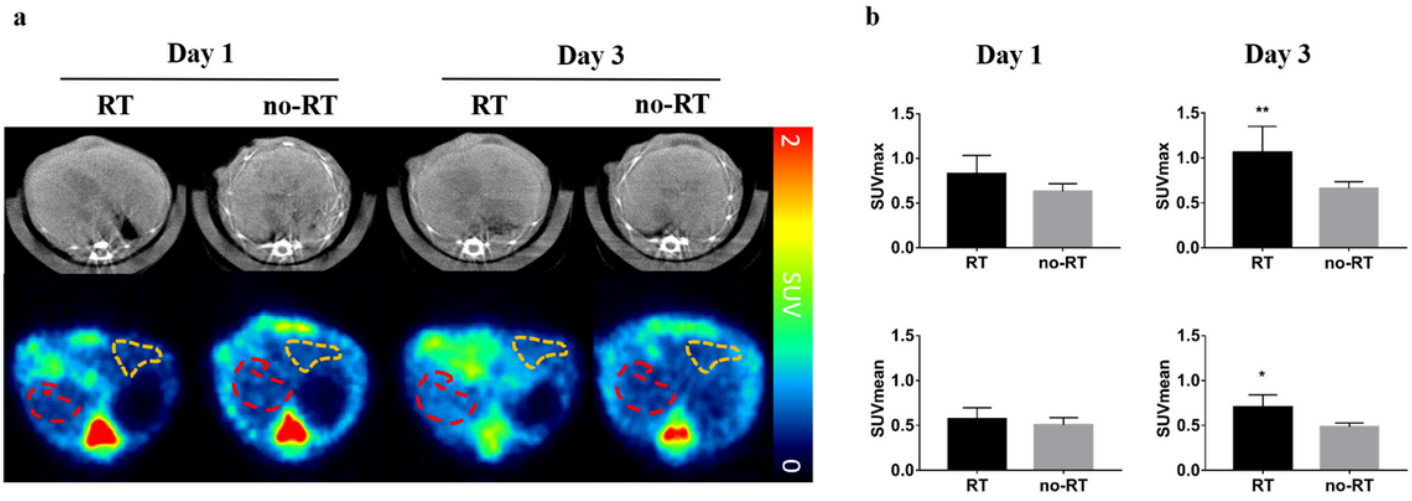

Figure 2

Impact of liver irradiation on 18F-FDG uptake by the areas surrounding orthotopic hepatocellular carcinomas in the right liver. Panel a: Representative transaxial images obtained in the RT and no-RT groups on the first and third post-irradiation days. Red and yellow dashed lines indicate the areas in the right and left liver lobes taken into account for the purpose of analysis. Panel b: SUVmean and SUVmax values measured in the right hepatic parenchyma on the first and third post-irradiation days. On the third post-irradiation day, both SUVmean and SUVmax values were significantly increased in the RT group – but not in the no-RT group.

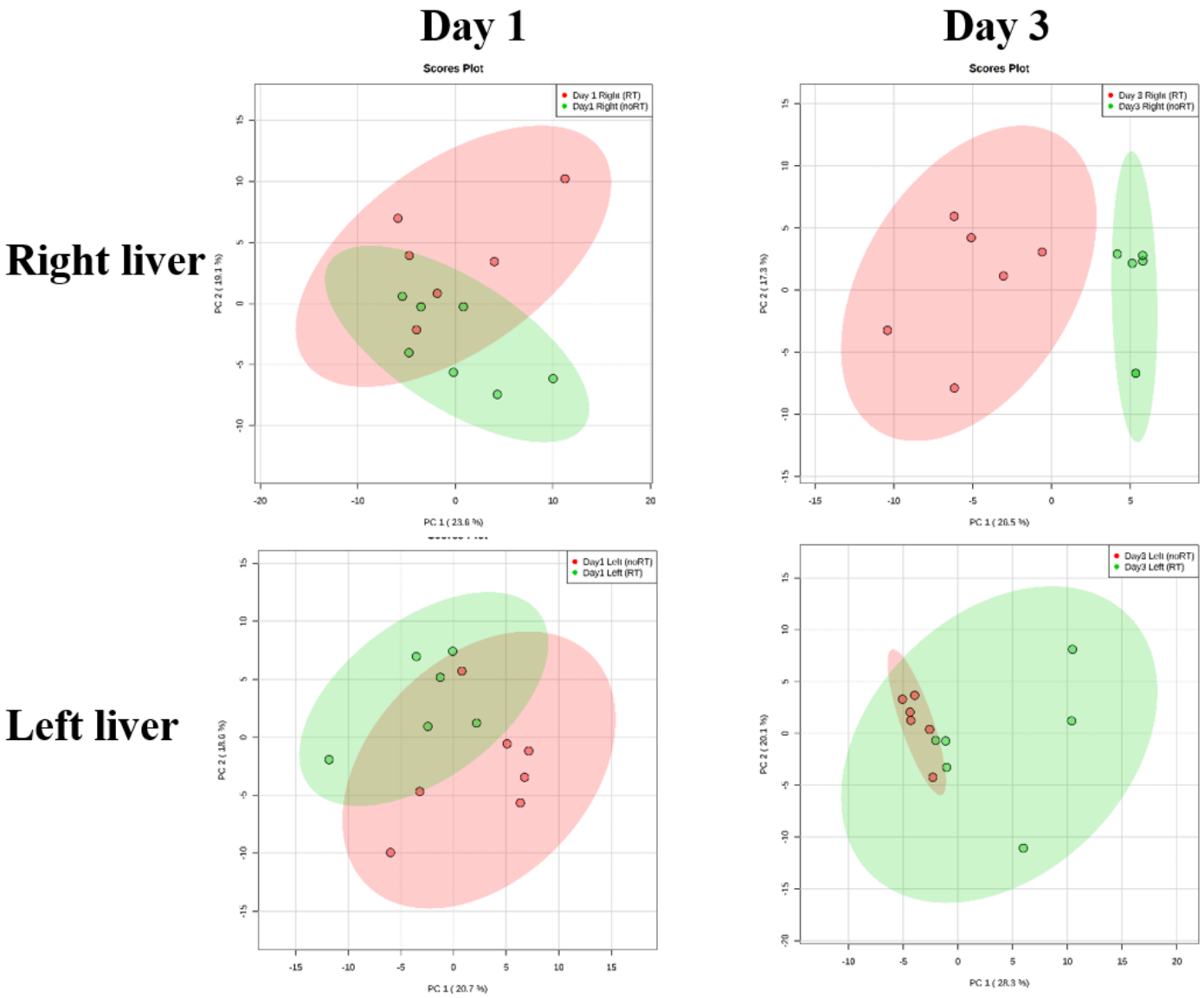

Figure 3

Principal component analysis of metabolite distribution in the RT and no-RT groups on the first and third post-irradiation days. Results are reported separately for the right and left lobes of the liver using partial least squares discriminant analysis. The areas (red for the RT group and green for the no-RT group) comprised within the elliptical rings indicate a 95% confidence level. A clear discrimination between the two experimental groups was observed for the right liver on the third post-irradiation day.

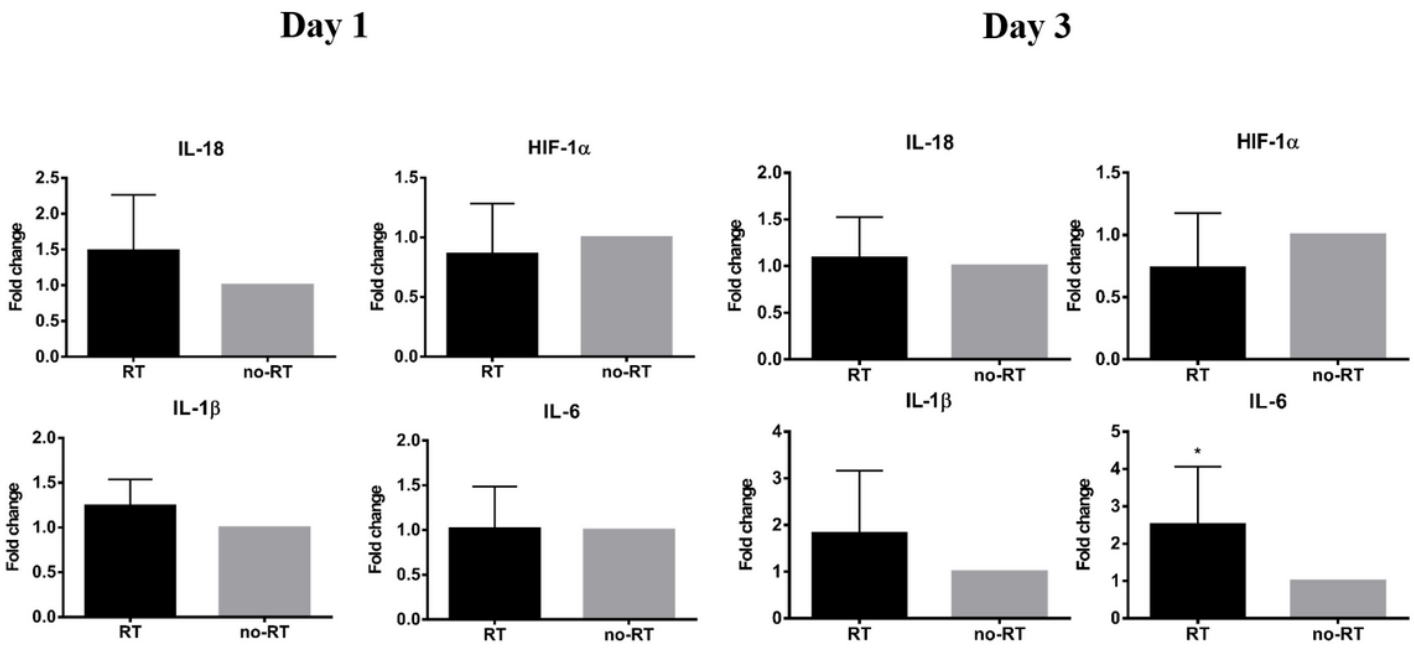

Figure 4

Expression levels of genes encoding for pro-inflammatory cytokines in the RT and no-RT groups on the first and third post-irradiation days (right lobe of the liver). On the third post-irradiation day, the expression levels of the IL-6 gene (expressed as fold-change) were significantly increased in the RT group – but not in the no-RT group.

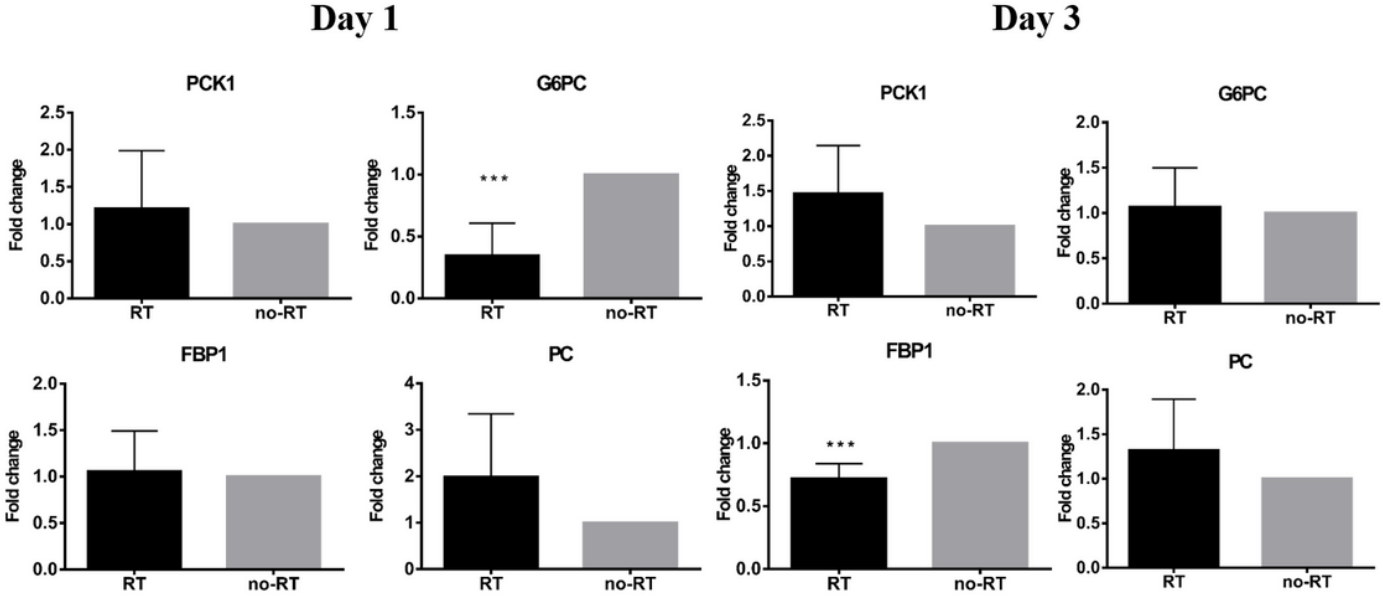

Figure 5

Expression levels of genes encoding for gluconeogenesis-associated enzymes in the RT and no-RT groups on the first and third post-irradiation days (right lobe of the liver). On the first post-irradiation day,

the expression levels of the G6PC gene (expressed as fold-change) were significantly lower in the RT group. On the third post-irradiation day, the expression levels of the FBP1 gene (expressed as fold-change) were significantly lower in the RT group. These results indicate the temporal shift from gluconeogenesis to glycolysis in the irradiated liver parenchyma.

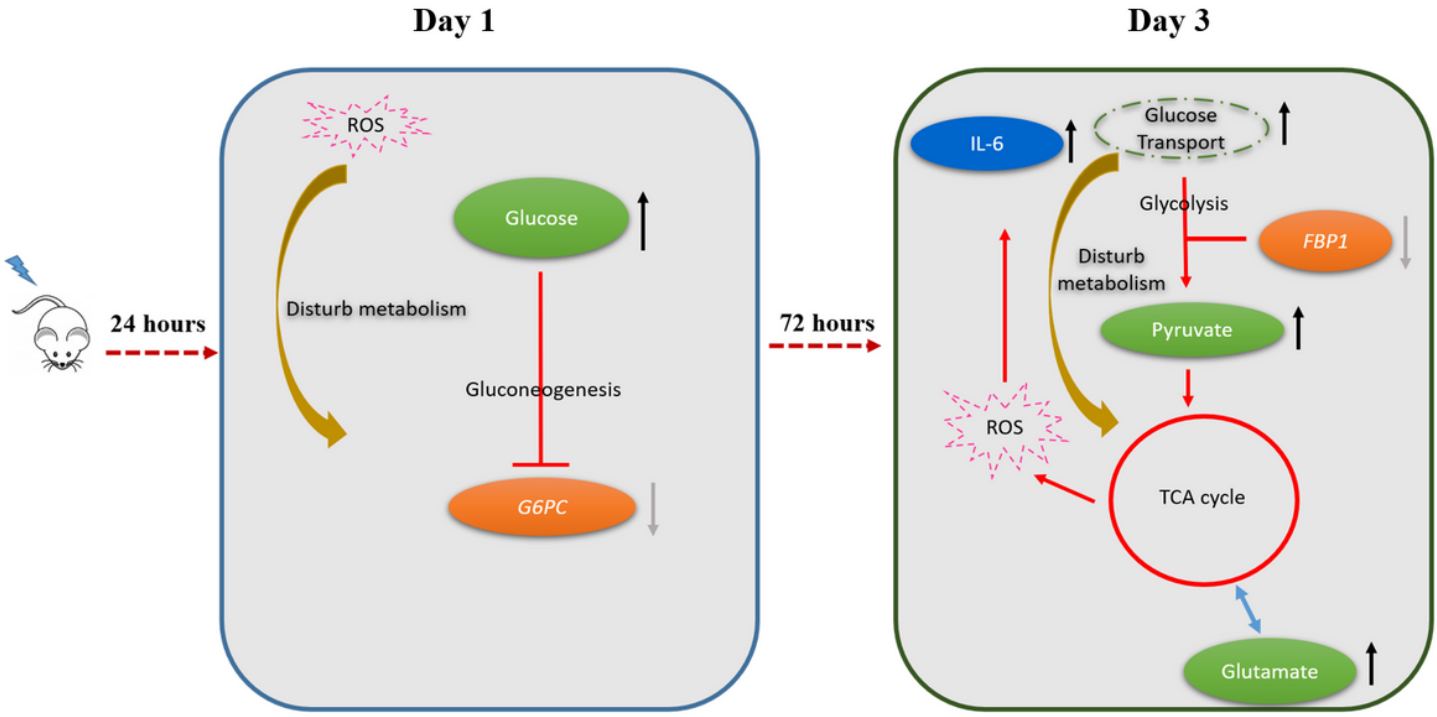

Figure 6

Shift in metabolic pathways from the first to the third post-irradiation day (right lobe of the liver). On the first post-irradiation day, radiation-induced production of reactive oxygen species (ROS) inhibited gluconeogenesis (as reflected by a reduced expression of the G6PC gene). On the third post-irradiation day, there was a shift towards glycolysis as reflected by a reduced expression of the FBP1 gene accompanied by an accumulation of pyruvate, glutamate, and the activation of the tricarboxylic acid cycle (TCA). The complex interplay between the activation of glycolysis and the presence of ROS also elicited an inflammatory response with an increased expression of IL-6. The metabolic shift occurring on day 3 can explain the significantly increased hepatic 18F-FDG uptake observed on 18F-FDG PET imaging at this time point.

Supplementary Files

This is a list of supplementary files associated with this preprint. Click to download.

- SUPPLEMENT.doc